Inorganica Chimica Acta 439 (2016) 82–91

Contents lists available at ScienceDirect

Inorganica Chimica Acta

journal homepage: www.elsevier.com/locate/ica

Bioactivity of new ferrocene incorporated N,N′-disubstituted ureas: Synthesis, structural elucidation and DFT study

Faiza Asghar [a,b], Amin Badshah [a,*], Bhajan Lal [c], Ian S. Butler [b], Saira Tabassum [d], Muhammad Nawaz Tahir [e]

[a] Coordination Chemistry Laboratory, Department of Chemistry, Quaid-i-Azam University, Islamabad 45320, Pakistan
[b] Department of Chemistry, McGill University, Montreal, QC H3A 2K6, Canada
[c] Department of Energy Systems Engineering, Sukkur Institute of Business Administration, Sukkur, Pakistan
[d] Department of Biotechnology, Faculty of Biological Sciences, Quaid-i-Azam University, Islamabad 45320, Pakistan
[e] Department of Physics, University of Sargodha, Sargodha, Pakistan

ARTICLE INFO

Article history:
Received 10 September 2015
Received in revised form 8 October 2015
Accepted 9 October 2015

Keywords:
Ferrocenyl ureas
DNA interaction
DFT
Antioxidant
Protein kinase inhibition
Antimicrobial

ABSTRACT

We report here the synthesis, structural characterization and biological assessment of three new ferrocene incorporated ureas (**1**–**3**). The synthesis of these complexes was accomplished by the deprotection of ferrocene-based thioureas to the corresponding oxo analogues using $NaOH_{(aq)}$ and mercuric chloride. The new ferrocenyl ureas were characterized by FT-IR, multinuclear (^{1}H and ^{13}C) NMR, AAS and elemental analysis. Furthermore, the single-crystal X-ray structure of compound **2** was also determined. The DNA binding potency of these ureas was evaluated by UV–Vis spectroscopy and cyclic voltammetry (CV). The three complexes interact electrostatically with DNA and have impressive binding constants ranging from 3.42×10^4 to $8.15 \times 10^4\ M^{-1}$. The diffusion coefficients of the drug–DNA adducts are lower than is that for the free drug indicating the formation of a high molecular weight complex that diffuses slowly towards the electrode. The small binding site size of 0.509 (**1**), 0.528 (**2**) and 0.473 (**3**) base pairs is also indicative of an electrostatic mode of interaction. The DFT calculated HOMO and LUMO energies correlate well with the experimentally determined redox potential values. The synthesized ureas (**1**–**3**) were screened for their antibacterial, antifungal and protein kinase inhibition potency. These compounds play a significant role in arresting microbial growth and are potent protein kinase inhibitors.

1. Introduction

The development of new anticancer and antimicrobial therapeutic agents is one of the fundamental goals in medicinal organometallic chemistry. Among the metallocenes, ferrocene has proved itself to be an excellent choice to design new drugs [1–3], most probably because of its small size, aromaticity, hydrophobicity, low cytotoxicity and redox behavior [4–7]. Moreover, ferrocene derivatives have already found significant uses as anticancer, antimalarial, antiviral and antibiotic agents [4]. DNA binding is a pre-requisite for a compound to be used as an antitumor agent. Some ferrocene derivatives have also been evaluated for their DNA binding affinity and display good DNA binding constants [8–12]. Generally, ferrocene derivatives interact electrostatically with DNA, but partial intercalation also has been reported [11]. Insertion of a ferrocene moiety into an organic compound not only improves the electrochemical and spectroscopic behavior but also augments the possible applications of the compound in which it is integrated by making it more lipophilic [13].

The urea group, $R_1R_2NCONR_3R_4$, is an attractive structural unit owing to its broad scope in bio-activities and is extensively found in natural products [14]. Consequently, urea derivatives have attracted considerable attention as anti-proliferative agents [15], anticancer (renal cancer, colon cancer, lungs cancer, prostate cancer and breast cancer) [16], anticonvulsant [17], antifungal [18] and antibacterial agents [19]. Aromatic urea derivatives, such as N-phenyl-N-(2-chloroethyl) urea and heterocyclic urea derivatives, show good anticancer activity due to their good inhibitory activity against receptor tyrosine kinases (RTKs) [20]. In addition, hydroxyurea has been investigated for the treatment of a wide range of solid tumors as well as acute and chronic leukemia [21]. Recently the N,N′-disubstituted urea functionality has received substantial attention as a moiety that is incorporated into the compounds with numerous biological activities and resultant therapeutic

* Corresponding author.
E-mail address: aminbadshah@yahoo.com (A. Badshah).

http://dx.doi.org/10.1016/j.ica.2015.10.007
0020-1693/

applications [22]. Inspired by the important applications of both ferrocene and ureas separately, we have combined them in a new class of molecules, i.e., ferrocene incorporated ureas.

We present here the synthesis, characterization and *in vitro* biological activities of three new ferrocene-based ureas. The drug–DNA binding activities of the three compounds have been determined by cyclic voltammetry (CV) and the proposed mode of interaction has been substantiated by UV–Vis spectroscopy. A density functional theory (DFT) study was also conducted on these structures to predict theoretically the redox potentials. In addition, we report here the antioxidant, protein kinase inhibition and antimicrobial activities of the compounds.

2. Experimental

2.1. Materials and methods

Ferrocene, 4-nitroaniline, HCl, $NaNO_2$, KSCN, $HgCl_2$, NaOH and acid chlorides such as *p*-bromobenzoyl chloride, *m*-bromobenzoyl chloride and *o*-bromobenzoyl chloride were obtained from Sigma Aldrich/Fluka and were used without further purification. All the solvents were dried and purified before use according to established methods. Para ferrocenyl aniline and ferrocene incorporated N,N′-disubstituted thioureas were synthesized by methods reported previously by our group (Part 1 Scheme 1) [11,23]. Melting points were determined in a capillary tube using an electrothermal melting point apparatus model MP-D Mitamura Riken Kogyo (Japan). NMR measurements were carried out on a Bruker AV 500 MHz spectrometer in DMSO using TMS (tetramethylsilane) as internal reference. FT-IR data was obtained on a Thermo Scientific NICOLET 6700 FT-IR instrument in the 4000–400 cm^{-1} range. Elemental analyses were performed using a LECO-932 CHNS analyzer, while the Fe concentrations were determined on Perkin–Elmer Atomic Absorption Spectrophotometer model 2380.

2.2. General procedure for synthesis of ferrocene incorporated N,N′-disubstituted ureas ***1–3***

To the solution of ferrocene incorporated N,N-disubstituted thioureas in 20 ml DMF, $HgCl_2$ was introduced in 1:1 molar ratio. The reaction mixture was stirred for 30 min, 3 mL of 100 mM $NaOH_{(aq)}$ was then added dropwise with constant magnetic stirring and the suspension was allowed to reflux for about 8 h. The progress of the reaction was monitored by thin layer chromatography (TLC). On completion of the reaction, the black precipitate of HgS were filtered off and the filtrate was then poured into ice cold water and stirred well in order to remove any water soluble impurities. The solid product was separated by filtration, washed with deionized water and recrystallized from ethanol (Scheme 1).

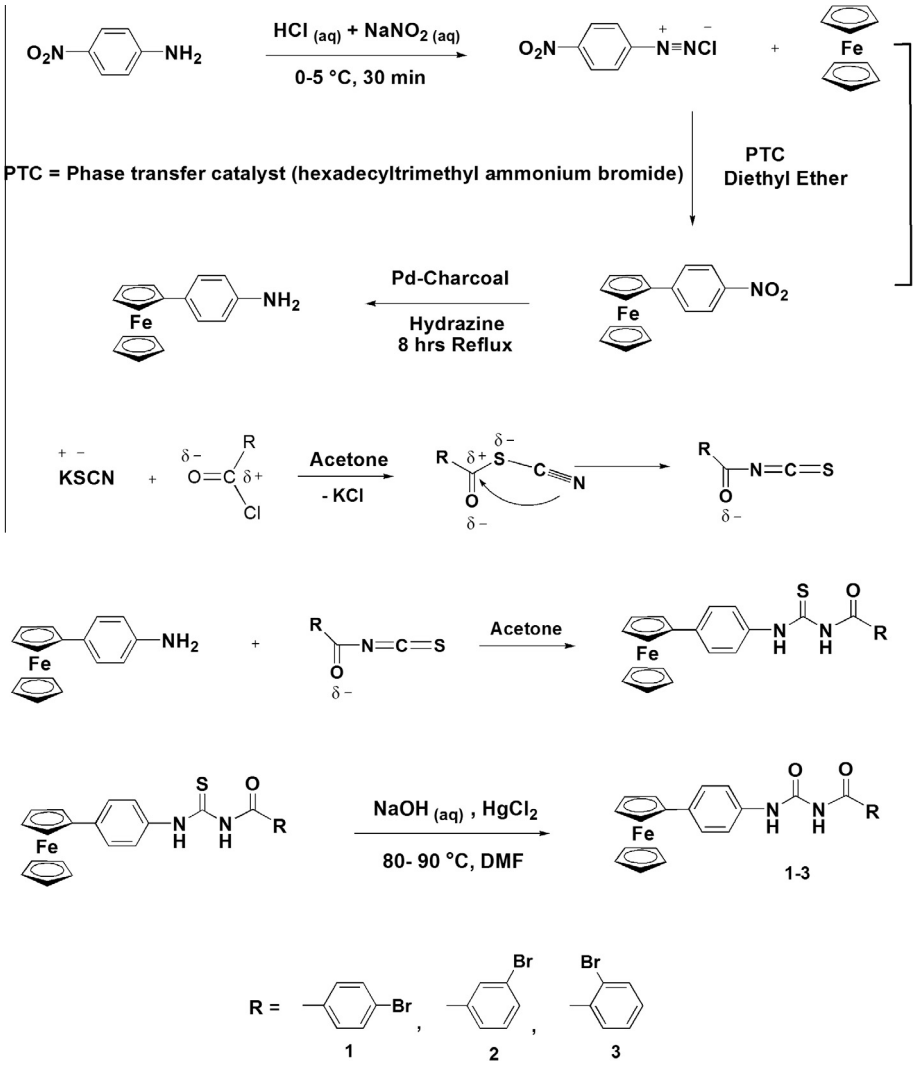

Scheme 1. Synthetic scheme for ferrocene incorporated N,N′-disubstituted ureas.

*2.2.1. 1-(4-Bromobenzoyl)-3-(4-ferrocenylphenyl)urea (**1**)*

Quantities used were 0.54 g (0.00107 mol) 1-(4-bromobenzoyl)-3-(4-ferrocenylphenyl) thiourea, 0.29 g (0.00107 mol) $HgCl_2$ and 3 ml of 100 mM $NaOH_{(aq)}$. Yield 75%; Brown solid; m.p. 173 °C; FT-IR (powder, cm^{-1}): 3338–3249 (N—H), 3091 (C—$H_{aromatic}$), 1697 (C=O), 1579 (C=C), 484 (Fe—Cp); ^{1}H NMR (500 MHz, DMSO-d^6, ppm) δ 11.67 (s, 1H, NH), 10.40 (s, 1H, NH), 7.87 (d, 2H, J = 8.0 Hz, ArH), 7.72 (d, 2H, J = 8.5 Hz, ArH), 7.20 (d, 2H, J = 8.0 Hz, ArH), 6.51 (d, 2H, J = 8.5 Hz, ArH), 4.58 (s, 2H, C_5H_4), 4.21 (s, 2H, C_5H_4), 3.98 (s, 5H, C_5H_5); ^{13}C NMR (125.81 MHz, DMSO-d^6, ppm) δ 167.1, 161.8, 147.5, 132.2, 131.8, 127.1, 125.7, 114.4, 87.5, 69.5, 68.2, 65.5; Elemental *Anal.* Calc. for $C_{24}H_{19}BrFeN_2O_2$: C, 57.28; H, 3.80; N, 5.58; Fe, 11.09. Found: C, 57.31; H, 3.77; N, 5.53; Fe, 11.08%.

*2.2.2. 1-(3-Bromobenzoyl)-3-(4-ferrocenylphenyl)urea (**2**)*

Quantities used were 0.54 g (0.00107 mol) 1-(3-bromobenzoyl)-3-(4-ferrocenylphenyl) thiourea, 0.29 g (0.00107 mol) $HgCl_2$ and 3 ml of 100 mM $NaOH_{(aq)}$. Yield 71%; Brown solid; m.p. 194 °C; FT-IR (powder, cm^{-1}): 3334–3244 (N—H), 3086 (C—$H_{aromatic}$), 1686 (C=O), 1591 (C=C), 483 (Fe—Cp); ^{1}H NMR (500 MHz, DMSO-d^6, ppm) δ 11.05 (s, 1H, NH), 10.47 (s, 1H, NH), 8.05 (s, 1H, ArH), 7.78 (d, 2H, J = 8.0 Hz, ArH), 7.64 (t, 2H, J = 7.5 Hz, ArH), 7.41 (d, 1H, J = 8.5 Hz, ArH), 7.20 (d, 2H, J = 8.0 Hz), 4.93 (s, 2H, C_5H_4), 4.40 (s, 2H, C_5H_4), 4.09 (s, 5H, C_5H_5); ^{13}C NMR (125.81 MHz, DMSO-d^6, ppm) δ 166.8, 160.6, 143.4, 137.4, 129.3, 127.7, 126.8, 125.3, 120.4, 116.9, 83.6, 70.4, 70.0, 67.2; Elemental *Anal.* Calc. for $C_{24}H_{19}BrFeN_2O_2$: C, 57.28; H, 3.80; N, 5.58; Fe, 11.09. Found: C, 57.26; H, 3.77; N, 5.55; Fe, 11.14%.

*2.2.3. 1-(2-Bromobenzoyl)-3-(4-ferrocenylphenyl)urea (**3**)*

Quantities used were 0.54 g (0.00107 mol) 1-(2-bromobenzoyl)-3-(4-ferrocenylphenyl) thiourea, 0.29 g (0.00107 mol) $HgCl_2$ and 3 ml of 100 mM $NaOH_{(aq)}$. Yield 62%; Yellow solid; m.p. 210 °C; FT-IR (powder, cm^{-1}): 3299–3230 (N—H), 3091 (C—$H_{aromatic}$), 1695 (C=O), 1589 (C=C), 477 (Fe—Cp); ^{1}H NMR (500 MHz, DMSO-d^6, ppm) δ 11.20 (s, 1H, NH), 10.42 (s, 1H, NH), 7.74–7.40 (m, 8H, ArH), 4.77 (s, 2H, C_5H_4), 4.33 (s, 2H, C_5H_4), 4.03 (s, 5H, C_5H_5); ^{13}C NMR (125.81 MHz, DMSO-d^6, ppm) δ 169.9, 160.1, 137.3, 135.8, 135.0, 133.2, 132.5, 129.4, 128.1, 126.8, 120.3, 119.1, 85.0, 69.8, 69.2, 66.5; Elemental *Anal.* Calc. for $C_{24}H_{19}BrFeN_2O_2$: C, 57.28; H, 3.80; N, 5.58; Fe, 11.09. Found: C, 57.25; H, 3.84; N, 5.61; Fe, 11.07%.

2.3. X-ray structure analysis

X-ray data for compound **2** were collected on a Bruker Kappa APEXII CCD diffractometer equipped with a graphite-monochromated Mo Kα (λ = 0.71073 Å) radiation source. Data collection used ω scans, and a multi-scan absorption correction was applied. The structure was solved using SHELXS-97 program. Final refinement on F^2 was carried out by full-matrix least squares using SHELXL-97 software [24].

2.4. DNA binding studies

2.4.1. Cyclic voltammetry

Voltammetric experiments were performed using a Biologic SP-300 voltammeter running with EC-Lab Express V 5.40 software, Japan. Analytical grade TBAP (tertiarybutylammonium perchlorate) was used as supporting electrolyte and N_2 gas (99.9%) was purged through the mixture to avoid any interference from oxygen. Commercial salmon DNA was solubilized in doubly distilled water to prepare a stock solution of 6×10^{-4} M from which working concentrations of DNA were prepared. The concentration of the stock solution was measured by UV absorbance at 260 nm using an epsilon value of 6600 M^{-1} cm^{-1}. For electrochemical measurements, a known concentration of the test solution was kept in an electrochemical cell and the voltammogram was recorded in the absence of DNA. The procedure was then repeated for systems with a constant concentration of the drug and varying concentrations of DNA. The working electrode was polished with alumina powder and rinsed with distilled water before every reading.

2.4.2. UV–Vis spectrophotometry

Absorption spectra were measured on a Shimadzu 1800 UV–Vis spectrophotometer. The absorption spectrum of a known concentration of the drug was recorded without DNA. The spectroscopic response was then monitored for the same amount of drug on addition of small aliquots of DNA solution. All samples were allowed to equilibrate for 15 min prior to each spectroscopic measurement.

2.5. DPPH scavenging activity

The reducing abilities of the compounds **1**–**3** were determined with the help of 1,1-diphenyl-2-picrylhydrazyl (DPPH) in DMSO to produce 1,1-diphenyl-2-picrylhydrazine. The decrease in the absorption of DPPH was monitored to calculate % age scavenging according to the following formula [10,25]:

$$\text{Scavenging Activity } (\%) = A_o - A/A_o \times 100$$

where A_o is the absorbance of free DPPH and A is the absorption of DPPH–drug mixture with an increasing concentration of drug. To a solution of DPPH (3.9 mg of DPPH in 100 ml DMSO) were added the increasing concentrations (12.5 μg/mL) of drug. The decrease in absorption of DPPH was monitored spectrophotometrically after 30 min at a wavelength of 517 nm. All the readings were taken in triplicate and the average of the readings was used.

2.6. DFT study

Computational studies were carried out for calculating the E_{HOMO} and E_{LUMO} orbitals of the compounds using DFT RB3LYP and 3-21G basis set. The density functional method (DFT) was used because of its simplicity and less time consumption [26]. Molecules were first optimized using DFT and energy calculations were performed on the optimized structures. Gaussian 03 W software was used for calculations.

2.7. Protein kinase inhibition assay

The kinase inhibition assay was performed using Streptomyces 85E strain according to the previously described protocol [27] with slight modification. The microorganisms under examination were first refreshed in a sterile Trypton soy broth (Merck, Germany) for 24–48 h and then applied to petri plates containing ISP4 minimal medium. Then, 6-mm Whatman filter paper discs soaked with 5 μL of each test sample (20 mg/mL DMSO) were employed on freshly seeded plates. Incubating the plates at 28 °C for 72 h was done to permit the growth of hyphae. The clear or bald zones around the disc, which indicate hyphae formation inhibition, were measured to the nearest mm with the help of a Vernier caliper. Surfactin served as the positive control, while DMSO impregnated discs were set as the negative control in order to confirm the non-toxic effect of DMSO.

2.8. Antimicrobial assay

2.8.1. Antibacterial study

Antibacterial activities of the synthesized ureas **1**–**3** were tested against five representative, gram-positive (*Staphylococcus aureus*,

Salmonella typhimurium, *Micrococcus luteus*) and gram-negative (*Bordetella bronchiseptica* and *Enterobacter aerogenes*) bacterial strains, by the disc diffusion method [28]. Prior to use, the bacterial isolates under investigation were first cultured in a nutrient broth for 18 h and standardized to 0.5 McFarland turbidity scale ($106\ cfu\ mL^{-1}$). The nutrient agar medium prepared by adding 2.3 g nutrient agar (MERCK) in 100 mL distilled water at pH 7.0 was autoclaved and then cooled up to 45 °C and seeded. Petri dishes in triplicate were prepared by introducing 75 mL of seeded nutrient agar medium and allowed to solidify. Wells were bored into the agar using a sterile 6 mm diameter cork borer. Approximately 100 μL each of the test compounds were infused into the wells, permitted to stand at room temperature for about 2 h and incubated at 37 °C. Controls were set in parallel in which the respective solvents were used to fill the well. Subsequent to the incubation of plates at 37 °C for 24 h, the diameter of zone of inhibition was measured. The effects were compared with penicillin (positive control) at a concentration of 1 mg/mL. The relative percentage inhibition of the tested compounds with respect to positive control was calculated by using the following formula:

$$\text{Relative percentage inhibition of the test compound} = 100 \times (X - Y)/(Z - Y)$$

where X is the total area of inhibition of the test sample, Y is the total area of inhibition of the solvent and Z is the total area of inhibition of the standard drug.

2.8.2. Antifungal study

The sensitivity of compounds **1**–**3** was tested against three different fungal strains, namely *Fusarium moniliforme*, *Aspergillus fumigatus* and *Aspergillus flavus*, using the agar tube dilution method [28]. Sample preparation was done by dissolving 2 mg of the compound in 1 mL of dimethyl sulfoxide (DMSO). In order to prepare the culture media, 6.5 g of sabouraud dextrose agar was dissolved per 100 mL distilled water (pH = 5.6). Next, 10 mL of the sabouraud dextrose agar (MERCK) was introduced into screw-capped tubes or cotton-plugged test tubes and autoclaved at 121 °C for 21 min. The tubes were cooled to 50 °C and sabouraud dextrose agar was loaded with 70 μL of the compound taken from stock solution. The tubes containing the media were then solidified in a slanting position at room temperature. For each fungal strain, three slants of test compounds were prepared. Tubes comprising the solidified media and test compounds were infused with a 4 mm diameter piece of inoculum, taken from a 7-day old culture of fungus. One test tube of each compound was prepared, which was used for positive control. Slants without compound were used for negative control. The test tubes were incubated at 28 °C for 7 days. During incubation, the cultures were examined twice a week. Readings were taken by measuring the linear length (mm) of the fungus in slant and growth inhibition was calculated with reference to the control. Percentage inhibition of fungal growth for each concentration of the compound was determined by using following formula:

$$\text{Percentage inhibition of fungal growth} = 100 - \frac{\text{Linear growth in test(cm)}}{\text{Linear growth in control(cm)}} \times 100$$

3. Results and discussion

3.1. Chemistry

Treating ferrocene-based thioureas with alkaline $HgCl_2$ in DMF yielded the ureas in good yield. The targeted compounds **1**–**3** were synthesized by the replacement of sulfur with oxygen [29] in the presence of alkaline Hg^{2+} as sulfur capturing agent. NaOH was used as an alkali which provides OH^- ion that attacks on thio-carbon of thiourea. The proposed mechanism comparable to that of guanylation is given in Scheme 3 [30].

3.2. Spectroscopic analysis

In the FT-IR spectra of the synthesized compounds, the two —NH protons gave a broad signal between 3374 and 3230 cm^{-1} attributable to intra and intermolecular hydrogen bonding. The stretch due to aromatic—H groups was evident just above 3000 cm^{-1} while the carbonyl group appeared as an intense band at 1697–1686 cm^{-1}. A characteristic peak for Fe—C associated with ferrocene group was observed in the range of 484–477 cm^{-1} for the compounds under study.

^1H and ^{13}C NMR spectra of the compounds were recorded in DMSO at room temperature. In the ^1H NMR spectra, all the compounds displayed two singlets for the two —NH protons. —NH proton which is present between two carbonyl carbons is maximum deshielded and provides a singlet at ~11 ppm. The second —NH which is attached to the phenyl ring is comparatively less deshielded, therefore it appears as a singlet at ~10 ppm. Five protons of unsubstituted cyclopentadiene (Cp) ring of ferrocene yielded an intense signal at ~4 ppm and substituted Cp provided two singlets downfield from the singlet of unsubstituted Cp ring. Aromatic protons were visible between 8 and 7 ppm. In the ^{13}C NMR spectra, maximum downfield carbon was between the two —NH groups with chemical shift value of 170–167 ppm. The other carbonyl carbon appeared at ~161 ppm because it was comparatively less deshielded. The Aromatic—C appears between 147 and 114 ppm. Unsubstituted Cp carbons of ferrocene gave an intense singlet whereas substituted Cp provided three peaks i.e. the ipso carbon appeared between 87 and 85 ppm and the other two signals were apparent between 70 and 65 ppm.

The elemental analyses of the compounds **1**–**3** were in good agreement with the calculated values, which demonstrates that the compounds are adequately pure in bulk.

Table 1
Crystal data of **2**.

	2
CCDC number	1062339
Empirical formula	$C_{24}H_{19}BrFeN_2O_2$
Formula weight	503.17
T (K)	296 (2)
λ (Å)	0.71073
a (Å)	12.5328 (7)
b (Å)	13.7905 (7)
c (Å)	14.5346 (7)
α (°)	111.901 (2)
β (°)	95.377 (3)
γ (°)	112.995 (2)
V (Å^3)	2059.54 (19)
Crystal system	triclinic
Space group	$P\bar{1}$
Z	4
D_{calc} (g/cm^3)	1.623
Index ranges	$-15 \leqslant h \leqslant 15$, $-17 \leqslant k \leqslant 17$, $-17 \leqslant l \leqslant 17$
Absorption coefficient (μ)	2.696
$F(000)$	1016
Goodness-of-fit (GOF) on F^2 (S)	1.030
Largest difference peak and hole (e Å^{-3})	0.81 and −0.60
Final R indices [I > 2sigma(I)]	$R_1 = 0.0411$, $wR_2 = 0.0914$
R indices (all data)	$R_1 = 0.0729$, $wR_2 = 0.1047$
θ range for data collection (°)	1.57–26

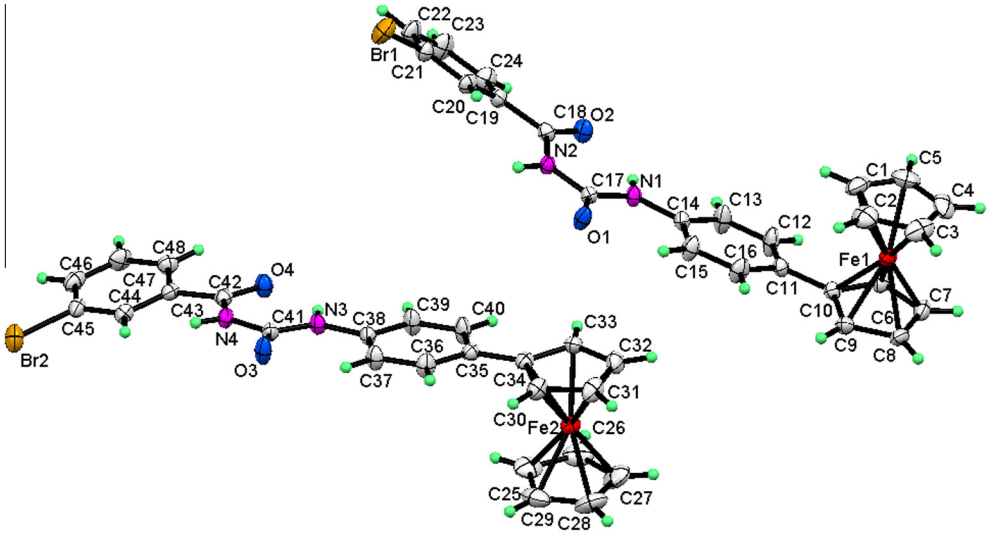

Fig. 1. Molecular diagram of **2** with ellipsoid displacement, non-hydrogen atoms represented by 30% probability boundary spheres and hydrogen atoms are sphere of arbitrary size.

Table 2
Selected bond lengths (Å) and angles (°) for **2**.

Bond lengths (Å)	
Br(1)—C(21)	1.896(4)
C(10)—C(11)	1.473(5)
N(1)—C(14)	1.416(4)
N(1)—C(17)	1.343(4)
N(2)—C(17)	1.395(4)
N(2)—C(18)	1.377(4)
O(1)—C(17)	1.222(4)
O(2)—C(18)	1.230(4)
N(1)—H(1A)	0.8600
N(2)—H(2A)	0.8600
C(18)—C(19)	1.490(5)
Bond angles (°)	
O(1)—C(17)—N(1)	125.4(3)
O(1)—C(17)—N(2)	118.6(3)
O(2)—C(18)—N(2)	122.3(3)
C(17)—N(1)—C(14)	126.7(3)
C(18)—N(2)—C(17)	129.5(3)
C(14)—N(1)—H(1A)	116.7
C(17)—N(2)—H(2A)	115.2
O(2)—C(18)—C(19)	122.1(3)
N(2)—C(18)—C(19)	115.6(3)
C(20)—C(21)—Br(1)	119.8(3)
C(22)—C(21)—Br(1)	119.5(3)

3.3. X-ray crystallography

Crystals of compound **2** suitable for crystallographic analysis were grown from dichloromethane/chloroform by slow evaporation. The results regarding data collection and structure refinement show that this compound crystallizes in a triclinic crystal system with $P\bar{1}$ space group. The basic crystal data and description of the diffraction experiment are given in Table 1. The molecular structure of **2** with numbering scheme is shown in Fig. 1, whereas selected bond lengths and bond angles are presented in Table 2. Intramolecular and intermolecular hydrogen bond interactions are summarized in Table 3 and shown in Fig. 2. The structural factors for the ferrocenyl substituent are within the usual range, and the iron atom is sandwiched almost perfectly centrally between the two cyclopentadienyl rings. For both the conformers, the distance of the iron atoms to the two cyclopentadienyl rings slightly differs. The variation in distances can be ascribed to close packing effect of two independent conformers. The structure reveals that the phenyl ring attached with ferrocene is exactly in plane with the Cp moiety but the bromo group present at the meta position of the other phenyl ring puts this ring out of the planar surface. Moreover, the ferrocene has adopted an eclipsed conformation. The pseudo six membered rings O2C18N2C17N1H1A and O4C42N4C41N3H3A are formed due to intra-molecular H-bonding, Reports from the literature prove that compounds with stronger non-bonding interactions have more capability to bind with macromolecules like proteins and DNA [11,31,32]. So, we expect a good association of **2** with DNA.

Table 3
The intramolecular and intermolecular hydrogen bond interactions in **2**.

H-Bonding	*D*	*H*	*A*	*d*(*D*–*H*) (Å)	*d*(*H*–*A*) (Å)	*d*(*D*–*A*) (Å)	*D*–*H*–*A* (°)
Intramolecular	N1	H1A	O2	0.86	2.00	2.690 (4)	136.6
	N3	H3A	O4	0.86	1.99	2.677 (4)	136.2
Intermolecular	N2	H2A	O3	0.86	1.95	2.790 (3)	166.8
	N4	H4A	O1	0.86	2.06	2.875 (3)	156.9

3.4. DNA binding studies

3.4.1. Cyclic voltammetry

Cyclic voltammetric (CV) measurements were performed with the objective of understanding the redox behavior and the DNA binding affinities of the synthesized ureas. The studies were carried out in a single compartment cell with a three-electrode configuration, i.e., working (platinum disc electrode with a geometric area of 0.071 $cm^2\ s^{-1}$), reference (saturated calomel electrode, i.e., SCE) and auxiliary electrodes (platinum electrode with geometric area much greater than working electrode) [33,34]. Changes in peak current provided information about the binding constants, while the mode of interaction of compound-DNA was judged from the variation in peak potential. Drug–DNA binding constants were calculated using the following equation [35]:

$$\log\ (1/[\mathrm{DNA}]) = \log\ K + \log\ (I/I_o - I) \quad (1)$$

where K is the binding constant, I and I_o are the peak currents with and without DNA. For determination of binding site size the following equation was used [36]:

$$C_b/C_f = K[\text{free base pairs}]/s \quad (2)$$

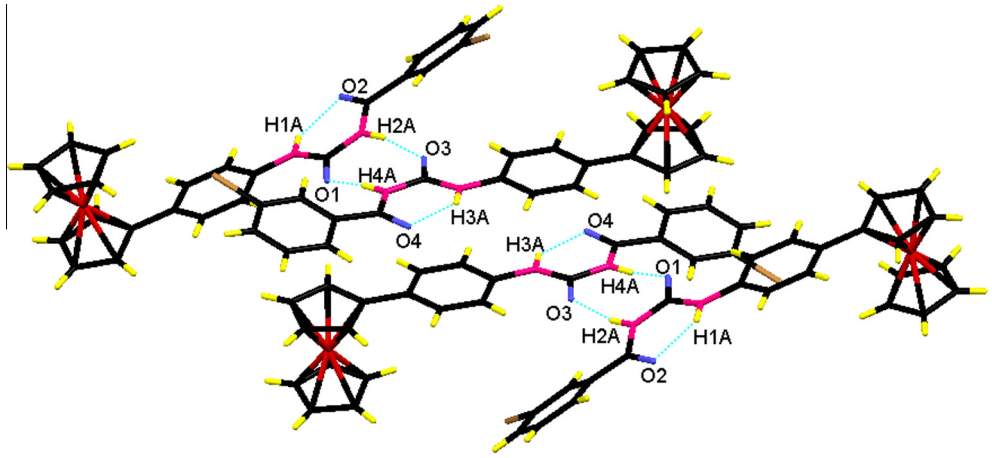

Fig. 2. Intermolecular and intramolecular hydrogen bonding in **2**.

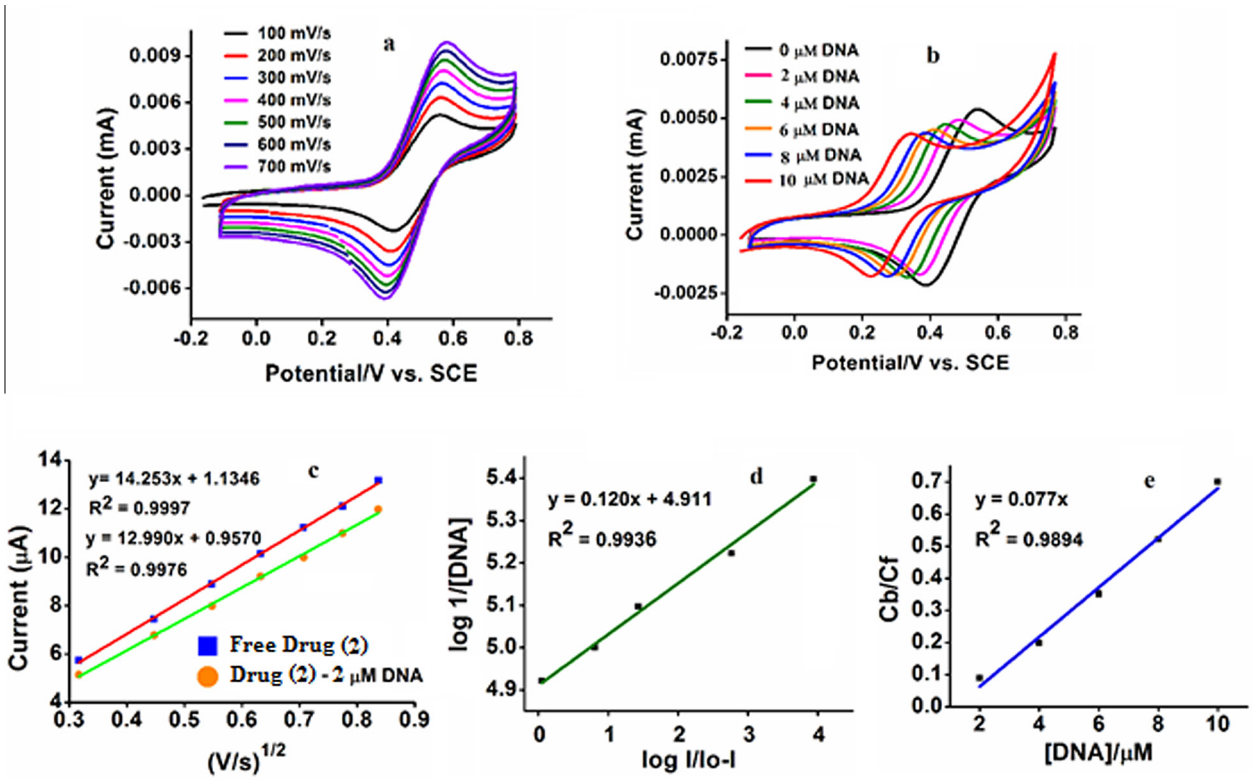

Fig. 3. (a) Representative plots of current vs. potential/V (SCE) at different scan rates for **2**. (b) Cyclic voltammogram of 1 mM **2** with 1 mL of 0.5 M TBAP as supporting electrolyte in the absence and presence of 2–10 μM DNA showing a decrease in I from I_o and a concentration dependent –ve shift in potential showing electrostatic interactions. (c) Representative plot of current vs. $(V/s)^{1/2}$, for the determination of diffusion coefficient of free drug (**2**) and drug (**2**)-2 μM DNA. (d) Representative plot of log $(I/I_o - I)$ vs. log (1/[DNA] for determination of binding constant of **2**. (e) Plot of C_b/C_f vs. [DNA]/μM for determination of binding site size of 2–10 μM DNA concentrations (**2**).

where s is the binding site size in terms of base pairs, K is the binding constant, C_b and C_f represents the concentration of free and drug–DNA bound species. If we consider the concentration of DNA in terms of nucleotide phosphate, then the concentration of DNA base pairs will be equal to [DNA]/2 and Eq. (2) can be written as:

$$C_b/C_f = K[\text{DNA}]/2s \quad (3)$$

and the value of C_b/C_f is equal [36] to $(I_o - I/I)$, which are the values of experimental peak currents. The diffusion coefficient of free drug and DNA-bound drug provides the best information about the molecular mass of the drug–DNA adduct. The following form of the Randles–Sevcik equation [37,38] was used for calculating the diffusion coefficients:

$$I_{pa} = 2.99 \times 10^5\ n\ (\alpha\ n)^{1/2} A C_o^* D_o^{1/2} v^{1/2} \quad (4)$$

where I_{pa} is the anodic peak current C_o^* is the concentration of the reductant (mol L^{-1}, A is the geometric area of the electrode in cm^2, n is the number of electrons involved in the process, D_o is the diffusion coefficient in $cm^2\ s^{-1}$.

The ferrocenyl ureas **1**–**3** show similar electrochemical behavior with two well-defined and stable redox peaks in the potential

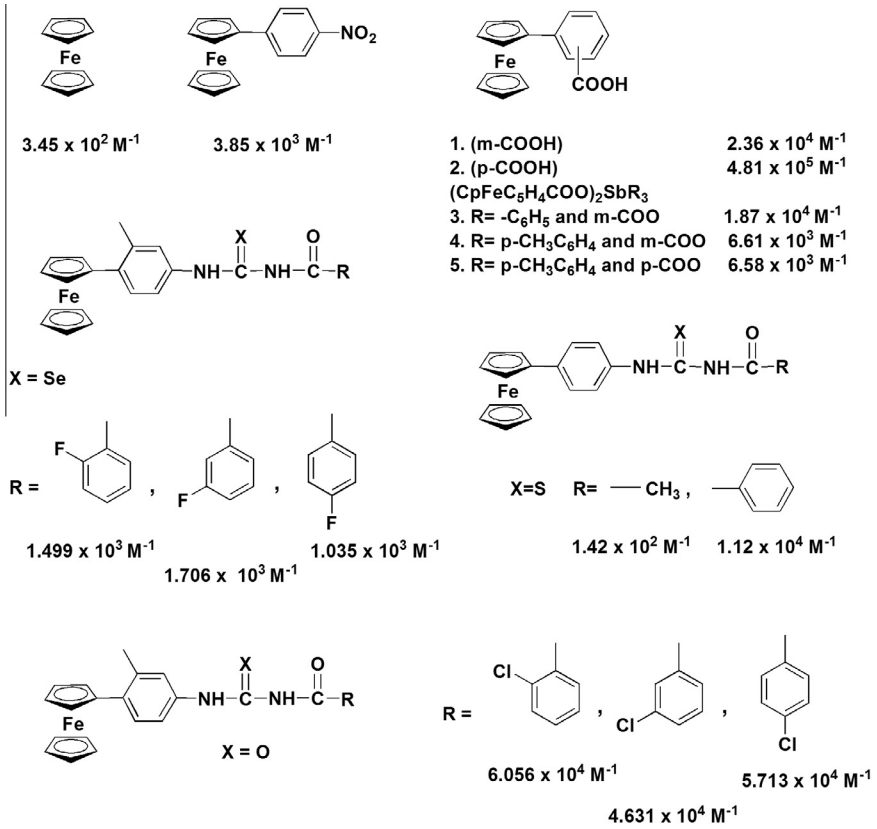

Scheme 2. Drug–DNA binding constants for ferrocene derivatives.

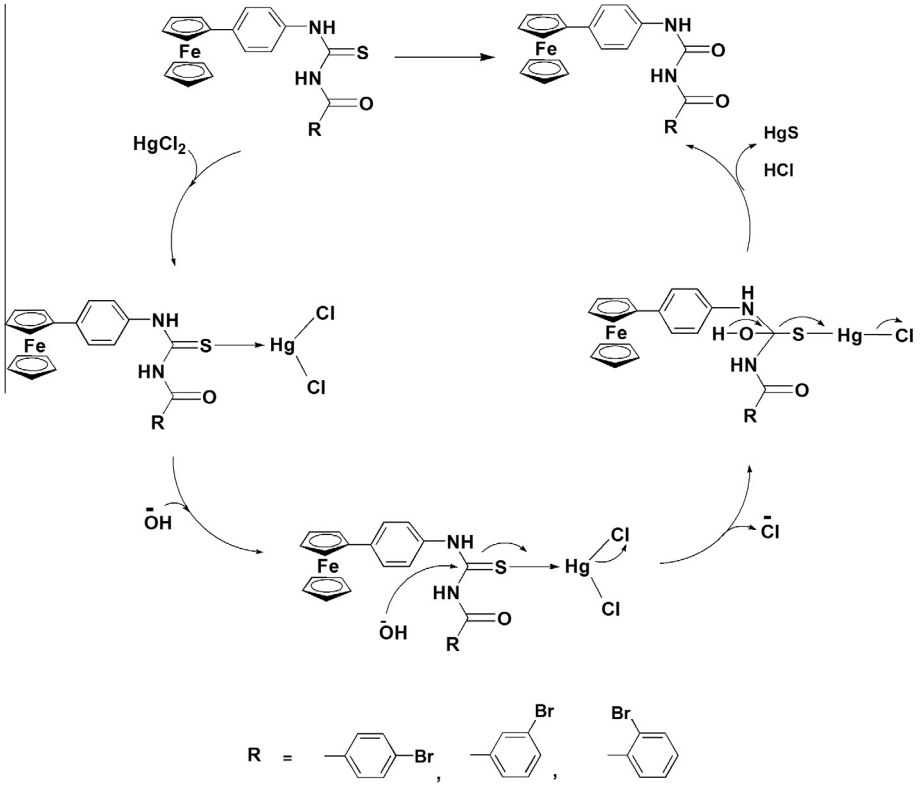

Scheme 3. Proposed mechanism for formation of ferrocene incorporated N,N′-disubstituted ureas.

Table 4
Important parameters for redox behavior and DNA binding studies (CV and UV).

Sample code	CV				UV
	K (M^{-1})	D_o ($cm^2\ s^{-1}$) Free drug	D_o ($cm^2\ s^{-1}$) drug–DNA	s (bp)	K (M^{-1})
1	6.828×10^4	6.65×10^{-7}	5.72×10^{-7}	0.509	7.769×10^4
2	8.147×10^4	6.14×10^{-7}	4.97×10^{-7}	0.528	9.316×10^4
3	3.424×10^4	5.13×10^{-7}	1.73×10^{-7}	0.473	5.225×10^4

range of −0.2–0.9 V. The consistency of the voltage at different scan rates from plots of current (mA) vs. potential (E/V vs. SCE) for the compounds favors quasi-reversible electrochemical process (Fig. 3a). The voltammogram of **2** provides an oxidation maximum at 0.602 V and reduction maximum at 0.483 V. With the addition of 2–10 μM DNA, a negative shift in the peak potential and a drop in the peak current is observed. This negative shift in potential justifies the probability of an electrostatic mode of interaction of the positively charged **2** with the negatively charged phosphate backbone of DNA. The decrease in current is attributed to the formation of a high molecular weight drug–DNA adduct, which diffuses comparatively slowly, thus causing a reduction in peak current [39] (Fig. 3b). The diffusion coefficient of the drug–DNA adduct is $4.23 \times 10^{-7}\ cm^2\ s^{-1}$ and this is far less than the diffusion coefficient of the free drug ($6.79 \times 10^{-7}\ cm^2\ s^{-1}$). This result indicates the slow diffusion of the high molecular weight drug–DNA adduct as compared to the free drug (Fig. 3c). The binding constant ($8.147 \times 10^4\ M^{-1}$) and binding site size (0.528 bp) were calculated using Eqs. (1) and (2) (Fig. 3d and e).

The drug–DNA binding constant was found to vary in the sequence: K_2 ($8.147 \times 10^4\ M^{-1}$) > K_1 ($6.828 \times 10^4\ M^{-1}$) > K_3 ($3.424 \times 10^4\ M^{-1}$). These binding constant values are far better than protonated ferrocene ($3.45 \times 10^2\ M^{-1}$) and are comparable with many of the recently reported ferrocene derivatives (Scheme 2) [8–11], which shows that the urea moiety is playing its part in the enhancement of binding constant. The small binding site size values of 0.509, 0.528 and 0.473 base pairs for compounds **1**, **2** and **3**, respectively, are also indicative of an electrostatic mode of interaction. Table 4 provides the important DNA binding parameters calculated by cyclic voltammetry.

3.4.2. UV–Vis spectroscopy

The results from CV were equally supported by UV–Vis spectroscopy in which a prominent hypochromism and a slight blue shift of the peak of the drug–DNA adducts relative to that of the free drug confirms the electrostatic interactions (Fig. 4a). A DNA binding constant of $9.316 \times 10^4\ M^{-1}$ for compound **2** is in close agreement with the value obtained from CV (Fig. 4b). The binding constant values are listed in Table 4.

3.5. DFT study

The reduction potentials of the compounds **1**–**3** measured from cyclic voltammetry revealed an analogous trend to that predicted from DFT studies. The ease of reduction of the compounds was found to vary in the following order: **2** > **3** > **1**. A similar trend was acquired from the E_{LUMO} values, i.e., the reduction potential of compound **2** was the highest owing to the easiest reduction and hence has the most negative E_{LUMO} value [40,41]. More negative E_{LUMO} favors addition of electrons as the energy of orbitals is reduced. The E_{HOMO} values obtained from DFT were compared with the oxidation potentials obtained from the CV measurements. The oxidation potentials observed experimentally for compounds **1**–**3** vary as **2** > **3** > **1**. This observation is supported from the DFT study by comparing the E_{HOMO} values, which is less negative for **1**, indicating its ease of oxidation as compared to other two (Fig. 6 and Table 5). A representative graphical demonstration of HOMO and LUMO orbitals of **2** is depicted in Fig. 5a and b.

3.6. DPPH scavenging activity

DPPH exhibits a strong absorption band at 517 nm due to its odd electron. When any antioxidant reacts with DPPH, it produces 1,1-diphenyl-2-picrylhydrazine. As a result the band intensity of DPPH decreases. This changes the color of DPPH and a corresponding decrease in the absorption. Fig. 7 shows a representative plot of absorbance versus wavelength for compound **2**. The IC_{50} values of 37.5, 62.5 and 50 μg/mL were determined for compounds **1**, **2** and **3**, respectively.

3.7. Protein kinase inhibition assay

Protein kinase inhibitors comprise a distinct class of oncogenic kinase inhibitors. Compounds **1**–**3** displayed a varying degree of inhibition with the zones of inhibition ranging from 16 ± 0.74 to 21 ± 1.02 mm. Compound **3** was found to be most effective as it produced the maximum zone of inhibition on the culture plates. The results of the inhibition assay revealed that the synthesized compounds can be considered as potential candidates to inhibit tumor initiation. The data from the inhibition study are given in Table 6.

3.8. Antimicrobial studies

All the compounds were screened for antibacterial and antifungal activities (Tables 7 and 8). The zone of inhibition values represent the mean value of the three readings with standard deviation. The activity of these compounds against different microbial strains is good but less than that of the standard drugs used. Compound **3** was found to be biologically most active as compared to **1** and **2**,

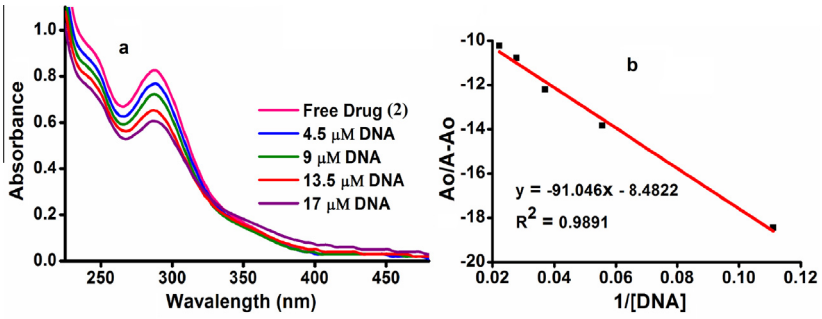

Fig. 4. (a) Representative plots of absorbance vs. wavelength of 25 μM **2** in ethanol with increasing concentration of DNA (4.5–17 μM). (b) Plot of $A_o/A - A_o$ vs. 1/[DNA] for determination of DNA binding constant of **2**.

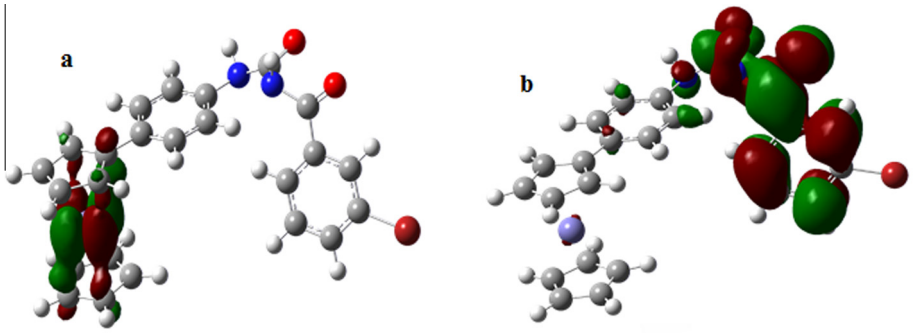

Fig. 5. (a) Representative graphical demonstration of HOMO of **2**. (b) Representative graphical demonstration of LUMO orbitals of **2**.

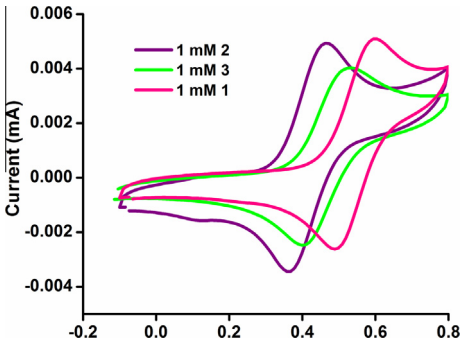

Fig. 6. Comparison of oxidation and reduction potentials of 1 mM ferrocenyl ureas **1**–**3** in DMSO recorded at a scan rate of 100 mV/s.

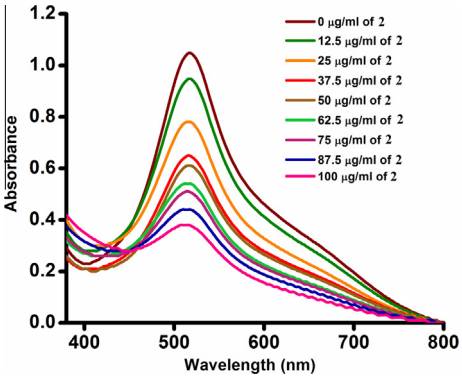

Fig. 7. Representative plots of absorbance vs. wavelength of **2** in DMSO for DPPH free radical scavenging activity.

Table 5
E_{HOMO} and E_{LUMO} values obtained through DFT calculations.

Sample code	E_{HOMO}	E_{LUMO}
1	−0.16341	−0.05802
2	−0.20586	−0.19685
3	−0.17981	−0.15566

Table 6
Protein kinase inhibition assay of ferrocenyl ureas.

Sample code	Zone of inhibition (mm)
1	17 ± 0.71
2	16 ± 0.74
3	21 ± 1.02
PC	25

PC = Surfactin was used as standard drug (positive control), while DMSO was used as negative control.

Table 8
In vitro antifungal activity of the ferrocenyl ureas and standard drug.

Sample code	*Fusarium moniliforme*		*Aspergillus fumigatus*		*Aspergillus flavus*	
1	3.33 ± 0.33[a]	68[b]	3.42 ± 0.03	67	3.11 ± 0.09	70
2	3.46 ± 0.03	64	4.48 ± 0.33	55	4.15 ± 0.33	60
3	2.47 ± 0.07	77	2.89 ± 0.06	73	2.05 ± 0.03	81
PC	0.77 ± 0.07	92	0.89 ± 0.03	92	0.83 ± 0.01	92
NC	10.3 ± 0.3	0	10.7 ± 0.03	0	10.3 ± 0.3	0

PC = Terbinafin (1 mg/mL) was used as standard drug (positive control), while DMSO was used as negative control (NC).
[a] Fungal growth (cm).
[b] Zone of inhibition (%).

probably due to more pronounced inductive effect of bromo group at ortho position than at the meta and para positions (inductive effect works up to three or four bonds). Due to electron withdrawing effect, a decrease in the basicity of NH and increase in lipophilicity may occur [42]. The decrease in basicity is due to less availability of the lone pair of electron to H-bond with water in the living cell (Scheme 4a and 4b).

Table 7
In vitro antibacterial activity of the ferrocenyl ureas and standard drug.

Sample code	*Staphylococcus aureus*	*Salmonella typhimurium*	*Micrococcus luteus*	*Bordetella bronchiseptica*	*Enterobacter aerogenes*
1	16.4 ± 0.60[a]	18.4 ± 0.67	17.6 ± 0.33	12.1 ± 0.67	13.8 ± 0.58
2	15.0 ± 0.33	16.1 ± 0.58	14.7 ± 0.58	11.3 ± 0.33	12.5 ± 0.33
3	18.7 ± 0.33	17.3 ± 0.58	21.1 ± 0.33	16.9 ± 0.70	17.7 ± 0.33
PC	26.7 ± 0.33	26.3 ± 0.33	27.3 ± 0.33	23.0 ± 0.58	20.3 ± 0.67

PC = Penicillin (1 mg/mL) was used as standard drug (positive control), while DMSO was used as negative control.
[a] Zone of inhibition in mm.

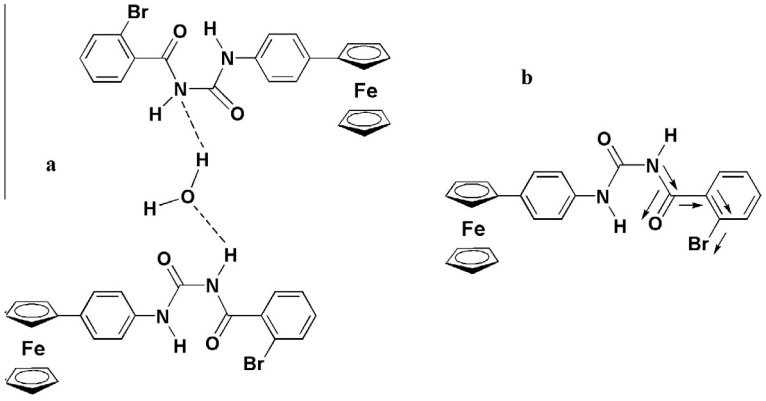

Scheme 4. (a) Hydrophilicity of ferrocenyl ureas. (b) Decrease in hydrophilicity and increase in lipophilicity by bromo group.

4. Conclusions

The ferrocenyl ureas **1**–**3** were successfully synthesized and characterized in good yields. These compounds were highly pure as characterized by several spectroscopic methods in the solid state as well as in solution. They are good DNA binders with binding constants varying in the sequence $K_2 > K_1 > K_3$. The preliminary antimicrobial screening data on these compounds reveals that these compounds are potential candidates for the effective control of such pathogens. These ferrocenyl ureas have also been demonstrated to be good candidates for protein kinase inhibition and free radical scavenging activity. These properties may prove valuable in the design of new anticancer and antimicrobial drugs.

Acknowledgements

Faiza Asghar is highly obliged to the Higher Education Commission (HEC) of Pakistan for providing a scholarship under the program 5000 Indigenous PhD Scholarships at Quaid-i-Azam University, Islamabad and for a 6-month scholarship under the International Research Support Initiative Program (IRSIP) as a Graduate Research Trainee in the Department of Chemistry, McGill University, Montreal, Quebec, Canada.

Appendix A. Supplementary material

CCDC 1062339 contains the supplementary crystallographic data for this paper. These data can be obtained free of charge from The Cambridge Crystallographic Data Centre via www.ccdc.cam.ac.uk/data_request/cif. Supplementary data associated with this article can be found, in the online version, at http://dx.doi.org/10.1016/j.ica.2015.10.007.

References

[1] M.F.R. Fouda, M.M. Abd-Elzaher, R.A. Abdelsamaia, A.A. Labib, Appl. Organomet. Chem. 21 (2007) 613.
[2] C. Ornelas, New J. Chem. 35 (2011) 1973.
[3] G. Gasser, N. Metzler-Nolte, Curr. Opin. Chem. Biol. 16 (2012) 84.
[4] B. Lal, A. Badshah, A.A. Altaf, N. Khan, S. Ullah, Appl. Organomet. Chem. 25 (2011) 843.
[5] (a) E. Hillard, A. Vessieres, L. Thouin, G. Jaouen, C. Amatore, Angew. Chem., Int. Ed. 45 (2006) 285;
(b) P. James, J. Neudorfl, M. Eissmann, P. Jesse, A. Prokop, H.G. Schmalz, Org. Lett. 8 (2006) 2763;
(c) G. Jaouen, S. Top, A. Vessieres, G. Leclercq, J.M. Mc, Curr. Med. Chem. 11 (2004) 2505.
[6] S.F. Forgues, B.D. Nicot, J. Photochem. Photobiol. A Chem. 132 (2000) 137.
[7] P. Nguyen, P.G. Elipe, I. Manners, Chem. Rev. 99 (1999) 1515.
[8] F. Asghar, A. Badshah, A. Shah, M.K. Rauf, M.I. Ali, M.N. Tahir, E. Nosheen, J. Organomet. Chem. 717 (2012) 1.
[9] F. Asghar, A. Badshah, R.A. Hussain, M. Sohail, K. Akbar, I.S. Butler, J. Organomet. Chem. 797 (2015) 131.
[10] R.A. Hussain, A. Badshash, M. Sohail, B. Lal, A.A. Altaf, Inorg. Chim. Acta 402 (133) (2013) 133.
[11] B. Lal, A. Badshah, A.A. Altaf, M.N. Tahir, S. Ullah, F. Huq, Dalton Trans. 41 (2012) 14643.
[12] S.E. Habas, H.A.S. Platt, M.F.A.M. van Hest, D.S. Ginley, Chem. Rev. 110 (2010) 6571.
[13] (a) C.G. Hartinger, P.J. Dyson, Chem. Soc. Rev. 38 (2009) 391;
(b) M.-G.A. Shvekhgeimer, Russ. Chem. Rev. 65 (1996) 41.
[14] K.M. Khan, S. Saeed, M. Ali, et al., Bioorg. Med. Chem. 17 (2009) 2447.
[15] M. Radić, S. Stojković, L. Marczi, I. Glavaš-Obrovac, Eur. J. Med. Chem. 45 (2010) 3281.
[16] E.L. Luzina, A.V. Popov, Eur. J. Med. Chem. 45 (2010) 5507.
[17] S.K. Kashawa, V. Kashawa, P. Mishra, N.K. Jain, J.P. Stables, Eur. J. Med. Chem. 44 (2009) 4335.
[18] R.H. Tale, A.H. Rodge, G.D. Hatnapure, A.P. Keche, Bioorg. Med. Chem. Lett. 21 (2011) 4648.
[19] P. Ventosa-Andrés, Á.M. Valdivielso, I. Pappos, M.T. García-López, N.E. Tsopanoglou, R. Herranz, Eur. J. Med. Chem. 58 (2012) 98.
[20] H.Q. Li, P.C. Lv, T. Yan, H.L. Zhu, Anticancer Agents Med. Chem. 9 (2009) 471.
[21] F. Fujita, M. Fujita, H. Inaba, T. Sugimoto, Y. Okuyama, T. Taguchi, Cancer Chemother. 18 (13) (1991) 2263.
[22] (a) A. Nefzi, M. Giulianotti, L. Truong, S. Rattan, J.M. Ostresh, R.A. Houghten, J. Comb. Chem. 4 (2002) 175;
(b) M.A.H. Ismail, S. Barker, D.A. El Ella, K.A.M. Abouzid, R.A. Toubar, M.H. Todd, J. Med. Chem. 49 (2006) 1526;
(c) A. Tizot, G.C. Tucker, A. Pierre, J. Hickman, S. Goldstein, Med. Chem. 5 (2009) 208;
(d) L. Zhu, J. Jin, C. Liu, C. Zhang, Y. Sun, Y. Guo, D. Fu, X. Chen, B. Xu, Bioorg. Med. Chem. 19 (2011) 2797.
[23] S. Ali, A. Badshah, A.A. Ataf, B. Lal, K.M. Khan, Med. Chem. Res. 22 (2013) 3154.
[24] G.M. Sheldrick, Acta Crystallogr. A64 (2008) 112.
[25] (a) S. Zouari, M. Ketata, N. Boudhrioua, E. Ammar, Ind. Crop Prod. 41 (2013) 172;
(b) A. Choudhary, R. Sharma, M. Nagar, M. Mohsin, H. Meena, J. Chil. Chem. Soc. 56 (2011) 911.
[26] S.J. Smith, B.T. Sutcliffe, Rev. Comput. Chem. 70 (1997) 271.
[27] G. Yao, F.M. Sebisubi, L.Y.C. Voo, C.C. Ho, G.T. Tan, L.C. Chang, J. Braz. Chem. Soc. 22 (6) (2011) 1125.
[28] (a) Atta-ur-Rahman, M.I. Choudhary, W.J. Thomesen, Bioassay Techniques for Drug Development, Harwood Academic Publishers, Amsterdam, 2001. 9–25;
(b) D. Kalemba, A. Kunicka, Curr. Med. Chem. 10 (2003) 813.
[29] S.G. Davies, A.A. Mortlock, Tetrahedron Lett. 32 (1991) 4791.
[30] C. Levallet, J. Lerpiniere, S.Y. Ko, Tetrahedron 53 (1997) 5291.
[31] F. Javed, A.A. Altaf, A. Badshah, M.N. Tahir, M. Siddiq, Z.U. Rehman, A. Shah, S. Ullah, B. Lal, J. Coord. Chem. 65 (2012) 969.
[32] C. Colovos, T.O. Yeates, Protein Sci. 2 (1993) 1511.
[33] M. Sirajuddin, S. Ali, A. Haider, N.A. Shah, A. Shah, M.R. Khan, Polyhedron 40 (2012) 19.
[34] A. Shah, A.M. Khan, R. Qureshi, F.L. Ansari, M.F. Nazar, S.S. Shah, Int. J. Mol. Sci. 9 (2008) 1424.
[35] Q. Feng, N.-Q. Li, Y.-Y. Jiang, Anal. Chim. Acta 344 (1997) 97.
[36] M. Aslanoglu, G. Ayne, Anal. Bioanal. Chem. 380 (2004) 658.
[37] A. Oliveira-Brett, J. Piedade, L. Silva, V. Diculescu, Anal. Biochem. 332 (2004) 321.
[38] A.M. Oliveira-Brett, V. Diculescu, J.A.P. Piedade, Bioelectrochemistry 55 (2002) 61.
[39] A. Shah, R. Qureshi, N.K. Janjua, S. Haque, S. Ahmed, Anal. Sci. 24 (2008) 1437.
[40] M. Marinov, S. Minchev, N. Stoyanov, G. Ivanova, M. Spassova, Croat. Chem. Acta 78 (2005) 9.
[41] B.W.D. Andrade, S. Datta, S.R. Forrest, P. Djurovich, E. Polikarpov, M.E. Thompson, Org. Electron. 6 (2005) 11.
[42] R. Gul, A. Khan, A. Badshah, M.K. Rauf, A. Shah, J. Organomet. Chem. 66 (11) (2013) 1959.